

Self-commissioning algorithm for matrix converter, nonlinearity compensation

*Original*

Self-commissioning algorithm for matrix converter, nonlinearity compensation / Yousefitalouki, Arzhang; Pellegrino, GIAN - MARIO LUIGI; Mengoni, Michele; Zarri, Luca. - (2015), pp. 4077-4083. ( Energy Conversion Congress and Exposition (ECCE), 2015 IEEE20-24 Settembre 2015) [10.1109/ECCE.2015.7310235].

*Availability:*

This version is available at: 11583/2635494 since: 2017-11-03T16:32:04Z

*Publisher:*

IEEE

*Published*

DOI:10.1109/ECCE.2015.7310235

*Terms of use:*

This article is made available under terms and conditions as specified in the corresponding bibliographic description in the repository

*Publisher copyright*

IEEE postprint/Author's Accepted Manuscript

©2015 IEEE. Personal use of this material is permitted. Permission from IEEE must be obtained for all other uses, in any current or future media, including reprinting/republishing this material for advertising or promotional purposes, creating new collecting works, for resale or lists, or reuse of any copyrighted component of this work in other works.

(Article begins on next page)

# Self-Commissioning Algorithm for Matrix Converter Nonlinearity Compensation

Arzhang Yousefi-Talouki, Gianmario Pellegrino

Dept. of Energy  
Politecnico di Torino  
Turin, Italy

Michele Mengoni, Luca Zarri

Dept. of Electrical, Electronic and Information Engineering  
University of Bologna  
Bologna, Italy

**Abstract**— Matrix converter nonlinear errors due to voltage drop and commutation delay introduce a distortion between voltage reference signals and output phase voltages. In current controlled applications, the current regulators are capable of compensating for such voltage command error. However, where output voltage estimation is required such as in state observers used for sensorless control of ac drives, the converter error reduces the accuracy of the voltage estimate, especially at low speeds. This work proposes a simple and accurate technique for the identification of converter parameters before the drive start-up. Based on the identified parameters, the nonlinearities are compensated. The feasibility and effectiveness of the presented method is shown in simulation. Experimental results are also reported.

**Keywords**—Matrix converter; self-commissioning; compensation of nonlinear errors.

## I. INTRODUCTION

Matrix converters (MCs) have emerged to become an attractive alternative to conventional ac-dc-ac converters [1-2]. These converters hold many advantages, including an adjustable input power factor, bidirectional power flow, high-quality power output waveforms and the lack of bulky capacitors [3-6].

In the literature, position sensorless control methods of ac motor drives have been sometimes associated to the use of the matrix converter [7-9]. Such control methods are based on flux linkage and position observers, requiring accurate knowledge of the voltage signals at the ac motor terminals. The use of command voltages instead of the measured ones is widely adopted, to reduce the cost of the hardware and improve the reliability of the system. However, it should be noted that this method causes an estimation error, consequence of the converter nonlinearities. This error is more evident at low speed. In recent years, different methods for eliminating the voltage command distortion produced by power converter nonlinearities have been developed for voltage source inverters (VSI) [10-11]. Such methods are based on offline identification. In [12], a self-commissioning algorithm has been proposed for the compensation of the inverter nonlinearities, which identifies the errors in the drive start-up, still for VSIs.

This paper proposes a self-commissioning algorithm for the identification and compensation of matrix converters voltage errors. Generally, two sources of voltage error exist in matrix converters. The first one is due to switching edge uncertainty (EU) due to commutation dead times, and the second one comes from the forward voltage drop (VD) of the power devices. The compensation technique proposed in [13] and implemented in the  $dq$  rotor synchronous frame cancels both EU and VD effects. The analytical model presented in [14] shows that the EU and VD effects tend to cancel each other. Moreover, the same work proposes a dual compensation technique in the  $\alpha$ - $\beta$  frame, with reference to four-step, current based commutation and double-sided switching pattern modulation. However, all mentioned methods need the knowledge of the parameters of the switches, resulting from the producer datasheets, the characteristics of the commutation sequence and switching pattern.

This paper proposes the commissioning of MC nonlinear errors before drive start-up without prior knowledge of power devices data and neither commutation pattern and commutation sequence. The indirect space vector technique [15] is used to modulate the output voltages and the input current vectors of the converter. Thus, the goal of this paper is the integration of MC self-commissioning and error model into the control of MC-supplied ac drives. The ultimate application of this method will be sensorless control of ac motor drives, and in particular synchronous reluctance motor drives.

## II. INDIRECT SPACE VECTOR MODULATION OF THE MATRIX CONVERTER

The power circuit topology of a three-phase matrix converter is shown in Fig.1. As other modulation techniques, Indirect Space Vector Modulation (ISVM) is used to synthesize the output voltage vector of MC, while imposing at the same time the phase of the input current vector. As depicted in Fig.2, in this modulation scheme, MC is separated into a fictitious voltage source rectifier (VSR) plus a voltage source inverter (VSI). The VSR controls the input current phase angle, whereas the VSI virtual stage generates the output voltage vector. Phase angles of measured input currents and output voltages are used to determine the sectors of the input current and output voltage vectors, respectively.

The input current and output voltage vector diagrams are shown in Fig. 3 under the assumption that the input current and

the output voltage vectors lie in sector 1. In both the VSR and VSI virtual stages, two adjacent vectors and one zero vector are used in order to produce a reference vector. For input sector 1, the virtual  $pn$  rail will switch between  $V_{AB}$ ,  $V_{AC}$  and zero. On the other hand, as shown in Fig.3 (b), the output voltage of the MC is synthesized switching between states  $pnn$ ,  $ppn$ , and zero of the virtual VSI.

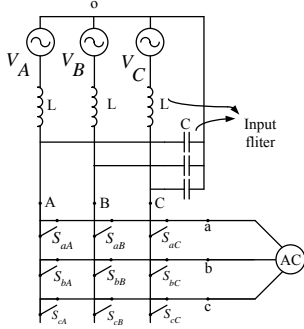


Fig. 1. Schematic diagram of a three-phase matrix converter.

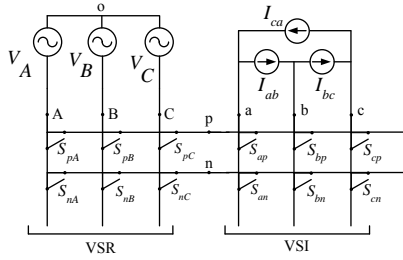


Fig. 2. Emulation of VSR and VSI conversion.

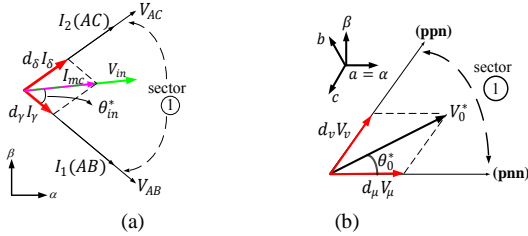


Fig. 3. ISVM, (a) rectification space vector modulation, (b): inversion space vector modulation.

For clarity,  $pnn$  means that the switches  $S_{ap}$ ,  $S_{bn}$  and  $S_{cn}$  in Fig. 2 are turned on. Therefore, combining VSI and VSR, there are five states per sector combination: ( $pnn$ -VAB,  $pnn$ -VAC,  $ppn$ -VAB,  $ppn$ -VAC, and zero). For example, in state  $pnn$ -VAB output phase-a is connected to the input phase-A, and output phases b and c are connected to the input phase-B. It is useful to define the directions of the input and output active vectors as  $\gamma, \delta$  for the VSR and  $\mu, \nu$  for the VSI. The respective duty cycles  $d_\gamma, d_\delta$  and  $d_\mu, d_\nu$  are graphically defined in Fig.3.

### III. MATRIX CONVERTER NONLINEAR ERRORS

The two sources of voltage errors in MCs are voltage drops of semiconductors and voltage edge uncertainty (EU) effect. These errors are briefly reviewed in the next sub-sections.

#### A. Voltage Edge Uncertainty Effect [14]

When a commutation is done in order to change the output phase voltage from one input phase to another one, a voltage is introduced which is dependent on commutation sequence and commutation patterns. In this work, four-step current-based commutation is adopted. Fig.4 shows the schematic diagram of a part of the MC consisting of the switches connecting input phases A and B to output phase a. Fig.5 shows the four-step commutation sequence when the output voltage changes from input phase A to input phase B, the output current is positive and  $V_A$  is greater than  $V_B$ . For details, see [16]. As can be seen from this figure, there is a voltage-time area error between the ideal output voltage  $V_a$  and the real one, which can be expressed as follows:

$$EU_{A \rightarrow B} = V_{AB}(t_{d1} + t_c + t_f). \quad (1)$$

where  $t_c$  is commutation time,  $t_f$  is IGBT falling time,  $t_{d1}$  and  $t_{d2}$  are the delay times for commutation.

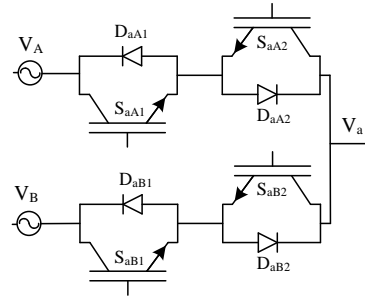


Fig. 4. Schematic diagram of a two-phase to single-phase matrix converter.

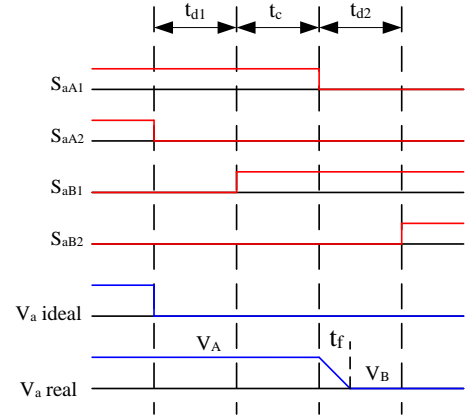


Fig. 5. Four-step current based commutation when output current is positive and input phase voltage  $V_A$  is more positive than  $V_B$ : commutation is from input phase A to input phase B.

Fig.6 shows a double-sided commutation pattern [17] for the output phase voltage  $V_a$  when the input phase voltage is in sector 1 and output current  $i_a$  is positive. If the switches are ideal IGBTs, the output voltage  $V_a$  is expressed by (2), where  $T_0$  is the timing of the zero vectors and  $T_{pwm}$  is the switching time.

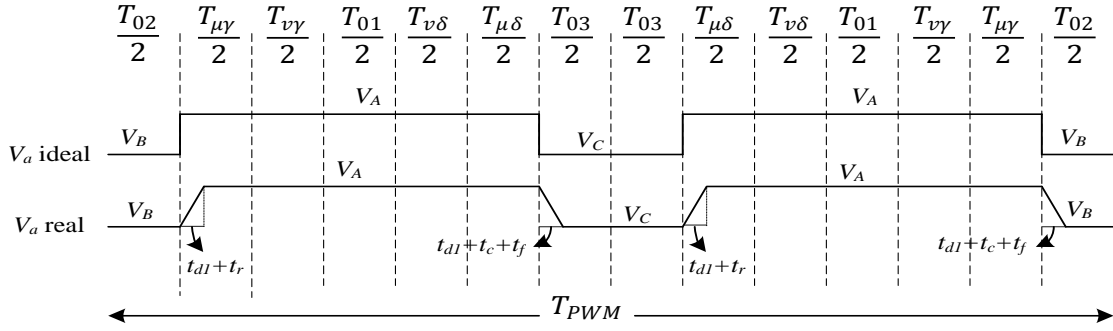


Fig. 6. Double-sided commutation pattern for output phase-a when the output current  $i_a$  is positive.

$$V_a = \frac{V_A(T_{PWM} - T_0)}{2T_{PWM}} \quad (2)$$

With real IGBT switches, the output voltage  $V_a$  is:

$$V_a = \frac{V_A(T_{PWM} - T_0)}{2T_{PWM}} + \frac{3V_A(t_c + t_f - t_r)}{T_{PWM}} \quad (3)$$

From (2) and (3) it is concluded that, when the input voltage vector is in sector 1 and the output current is positive, EU effect adds a term to the output voltage, and vice versa when output phase current is negative (4).

$$EU_a = \frac{3V_A(t_c + t_f - t_r)}{T_{PWM}} \cdot \text{sign}(i_a). \quad (4)$$

As can be seen from Fig.7, the input voltage  $V_A$  varies in sector 1 between a minimum value  $\frac{\sqrt{3}}{2} V_{pk}$  and peak value  $V_{pk}$ . Thus, the EU voltage error expressed in (4) varies between a maximum and minimum value, as depicted in Fig.8, according to the phase angle of the input voltage within the considered sector. Expressions similar to (4) are valid for the other output phases  $b$  and  $c$ , and for input voltage sectors other than #1. In general:

$$EU_i = \frac{3V_j(t_c + t_f - t_r)}{T_{PWM}} \cdot \text{sign}(i_i), \quad j = A, B, C, \quad i = a, b, c. \quad (5)$$

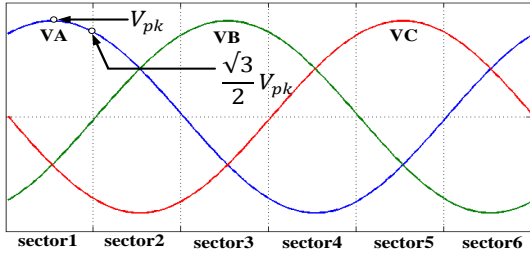


Fig. 7. Input phase voltages and corresponding sectors.

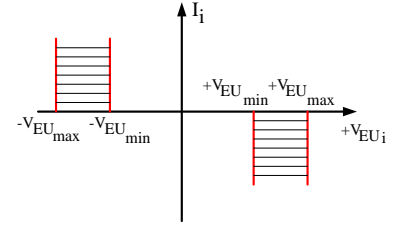


Fig. 8. Voltage edge uncertainty effect.

The voltage EU error introduced by different input sectors is tabulated in Table I.

TABLE I. EDGE UNCERTAINTY ERROR EFFECT FOR THE DIFFERENT INPUT SECTORS

Input sector	$V_{EU}$
1	$3V_A \frac{t_c + t_f - t_r}{T_{pwm}} \text{sign}(I_i); \quad i = \{a, b, c\}$
2	$3V_C \frac{t_c + t_f - t_r}{T_{pwm}} \text{sign}(I_i); \quad i = \{a, b, c\}$
3	$3V_B \frac{t_c + t_f - t_r}{T_{pwm}} \text{sign}(I_i); \quad i = \{a, b, c\}$
4	$3V_A \frac{t_c + t_f - t_r}{T_{pwm}} \text{sign}(I_i); \quad i = \{a, b, c\}$
5	$3V_C \frac{t_c + t_f - t_r}{T_{pwm}} \text{sign}(I_i); \quad i = \{a, b, c\}$
6	$3V_B \frac{t_c + t_f - t_r}{T_{pwm}} \text{sign}(I_i); \quad i = \{a, b, c\}$

### B. Voltage Drop Effect

The voltage drop effects in a MC can be modeled with a simplified linearized model [9]. As in MC two devices are always conducting, the voltage drop across the power devices is modeled as (6), where  $V_{th}$  is the forward voltage of power device that is approximated by a fixed threshold value. The threshold

voltage  $V_{th}$  includes the average effect of one diode and one IGBT, whereas  $R_d$  accounts for two devices in series.

$$V_{Di} = 2V_{th} \text{sign}(I_i) + R_d I_i, \quad i = \{a, b, c\}. \quad (6)$$

### C. Overall Matrix Converter Voltage Error

The voltage drop error and voltage edge uncertainty error have similar effects on converter voltage, but opposite in sign. The EU error adds an extra voltage-time area to the output voltage when the output current is positive, whereas the device voltage drop subtracts voltage to the output. The overall voltage is obtained by summing the voltage EU resulting from table I and the voltage drop from (6), as follows:

$$V_{error,i} = V_i^* - V_i = V_{Di} - 3V_j \frac{t_c + t_f - t_r}{T_{pwm}} \text{sign}(I_i). \quad (7)$$

Where  $j = \{A, B, C\}$ ,  $i = \{a, b, c\}$ .

Edge uncertainty and forward voltage effects can be compacted into a single nonlinear term of amplitude  $V'_{th}$  as expressed in (8). As can be seen, the overall voltage consists of a nonlinear part and a linear part. The equivalent threshold voltage  $V'_{th}$  includes the effects of EU and VD.

$$V_{error} = V'_{th} \text{sign}(I_i) + R_d I_i. \quad (8)$$

$$V'_{th}(6\vartheta_i) = 2V_{th} - 3V_j(6\vartheta_i) \frac{t_c + t_f - t_r}{T_{pwm}}, \quad j = \{A, B, C\}. \quad (9)$$

The device resistance  $R_d$  is in series with the stator resistance  $R_s$ , whereas the argument  $6\vartheta_i$  refers to the sector of input voltage as depicted in Fig.9.

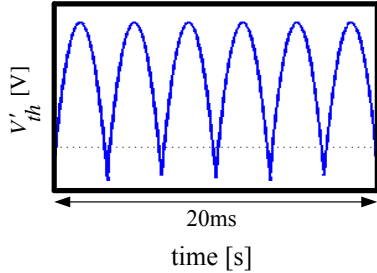


Fig. 9. Equivalent threshold voltage in one period of the 50 Hz input voltage.

## IV. IDENTIFICATION AND COMPENSATION OF MATRIX CONVERTER VOLTAGE ERRORS

This procedure is done through two successive tests based on direct current (dc) supply of the load. When a direct current is injected into the motor at standstill, the back-emf is zero and therefore, the converter phase load is the total resistance  $R_s + R_d$ , where  $R_s$  accounts for motor stator resistance and  $R_d$  for the converter power devices. Based on this assumption, two consecutive dc steps are used to identify the converter nonlinearities. The dc pulses are applied to the  $\alpha$  axis of the motor (i.e. the phase- $a$  axis) via the  $dq$  current controllers.

### A. Identification of Total Resistance $R_s + R_d$

Initially, the current  $I_{\alpha 1}$  is injected in the motor at stand-still by means of a closed-loop control system. Taking into account

the converter error, the reference voltage on  $\alpha$  axis at steady state is:

$$v_{\alpha 1}^*(6\vartheta_i) = V'_{th}(6\vartheta_i) + (R_s + R_d) I_{\alpha 1}. \quad (10)$$

Later, when a second dc current  $I_{\alpha 2}$  is injected along the same axis, the reference voltage will be:

$$v_{\alpha 2}^*(6\vartheta_i) = V'_{th}(6\vartheta_i) + (R_s + R_d) I_{\alpha 2}. \quad (11)$$

Thus, using (10) and (11),  $R_d + R_s$  can be calculated by (12)

$$R_s + R_d = \frac{v_{\alpha 2}^*(6\vartheta_i) - v_{\alpha 1}^*(6\vartheta_i)}{I_{\alpha 2} - I_{\alpha 1}}. \quad (12)$$

provided that (11) is applied for the same  $\theta_i$ . Alternatively, reference voltages can be time-averaged to obtain a consistent subtraction of the two voltage levels:

$$R_s + R_d = \frac{v_{\alpha 2,avg}^* - v_{\alpha 1,avg}^*}{I_{\alpha 2} - I_{\alpha 1}}. \quad (13)$$

### B. Identification of the Pole Error Voltage ( $V'_{th}$ )

After the calculation of  $R_d + R_s$ , the pole error voltage can be easily calculated using (10) or (11). The pole voltage error, averaged with respect to input phase angle, is:

$$V'_{th,avg} = v_{\alpha 2,avg}^* - (R_s + R_d) I_{\alpha 2}. \quad (14)$$

The control scheme used for the self-commissioning of the matrix converter is shown in Fig.10.

### C. Feedforward Compensation based on Signum Function

The total voltage error ( $V_{EU} + V_D$ ) is feedforward compensated, as depicted in Fig.11. The phase voltages are evaluated according to the signum of the output phase currents and the three-phase voltage compensation signals are transformed into two-phase components in the  $\alpha$ - $\beta$  stator reference frame, and added to the output of the current regulators.

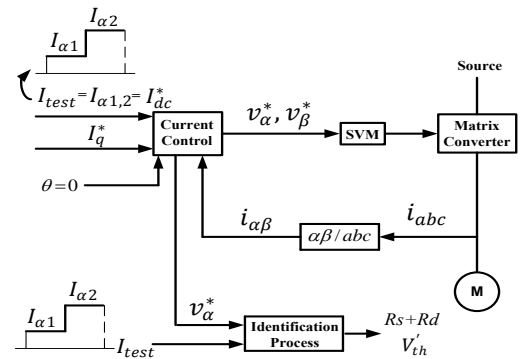


Fig. 10. Control schematic for self-commissioning of matrix converter.

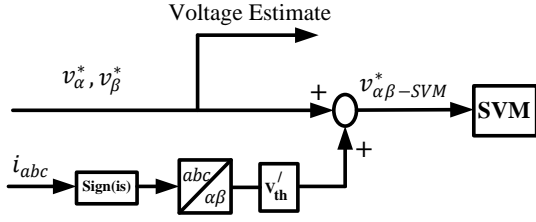


Fig. 11. Feedforward compensation for matrix converter nonlinearity.

## V. SIMULATION AND EXPERIMENTAL RESULTS

The self-commissioning procedure has been verified firstly in simulation for a 2.2 kW synchronous reluctance motor and then in experiments for a 2.2 kW induction motor. Synchronous reluctance and induction motors ratings are summarized in Tables II and III, respectively. Also, key data of the matrix converter under test are tabulated in table IV.

TABLE II. SYNCHRONOUS RELUCTANCE MOTOR SPECIFICATION

Rated power/Number of poles	2.2 kW / 4
Nominal Speed/Rated Torque	1500 rpm / 14 Nm
Stator resistance	4.34 $\Omega$

TABLE III. INDUCTION MOTOR SPECIFICATION

Rated power/Number of poles	2.2 kW / 4
Nominal Speed/Rated Torque	1430 rpm / 14.7 Nm
Stator resistance	2.85 $\Omega$

TABLE IV. MATRIX CONVERTER SPECIFICATION

EUPEC FM35R12KE3ENG module	
Power devices	1200 V, 35 A, IGBT
$t_c$	0.3 $\mu s$
$t_f / t_r$	65-90 ns / 30-45 ns

The simulation results are presented in two parts. The first part refers to the error identification process. In the next part, results related to the compensation method and its effectiveness are presented. In the simulations, the input phase voltage of matrix converter is 400 V.

### A. Identification of MC Voltage Error

As described in section IV, two dc pulses with different amplitudes,  $I_{\alpha 1} = 2$  A and  $I_{\alpha 2} = 4$  A, are injected into the SyR motor. The first dc current is injected in the time interval 0 – 0.3 s and the second one is applied in time interval 0.3 - 0.6 s, as shown in Fig.12. For the first test,  $v_{\alpha 1}^*$  is sampled and averaged from  $t=0.1$  s to  $t=0.3$  s and for the second test,  $v_{\alpha 2}^*$  is sampled and averaged in the period 0.4-0.6 s, as depicted in Fig.13. It can be seen from this figure that,  $v_{\alpha 1,avg}^*$  is ready at 0.3 s and  $v_{\alpha 2,avg}^*$  is ready at 0.6 s.

The values of  $R_d + R_s$  and  $V_{th}'$  are identified through (13) and (14) as illustrated in Figs.14 and 15. The value 4.59  $\Omega$  is found for  $R_d + R_s$ . The average value of actual threshold voltage  $V_{th}'$  of the considered converter is approximately -1.9 V as shown in Fig.15. The negative value of identified  $V_{th}'$  means

that the edge uncertainty effect is more important than the voltage drop effect.

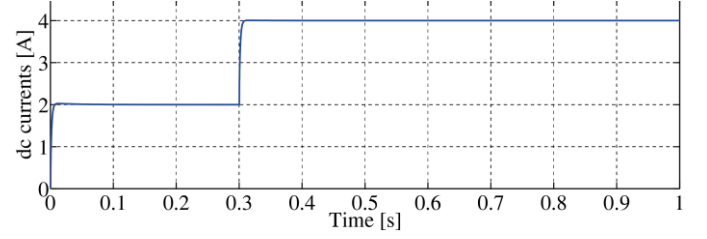


Fig. 12. Injected dc currents ( $I_{\alpha 1}$  &  $I_{\alpha 2}$ ).

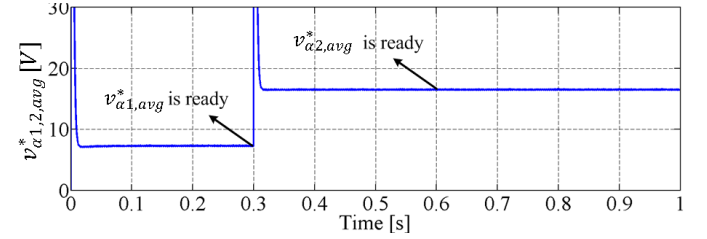


Fig. 13.  $v_{\alpha 1}^*$  and  $v_{\alpha 2}^*$  during the injection of  $I_{\alpha 1}$  &  $I_{\alpha 2}$ .

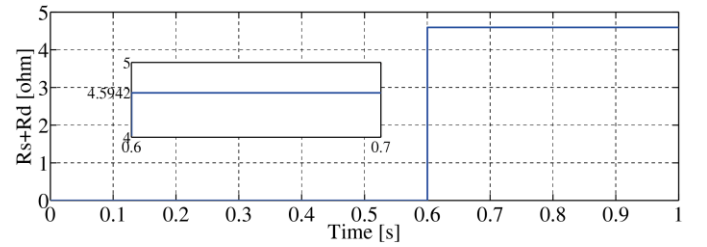


Fig. 14. Identification of overall resistance ( $R_s + R_d$ ).

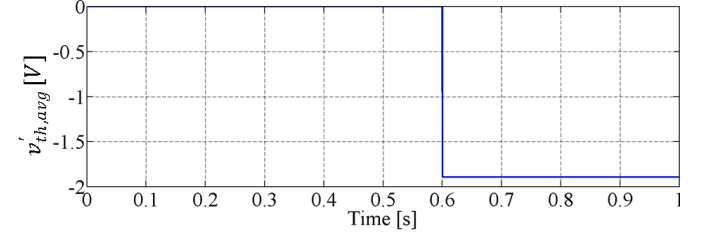


Fig. 15. Identification process for threshold voltage error.

### B. Compensation of MC Voltage Error

Then, comparative results with and without voltage error compensation are presented. The motor speed is kept at 15 rpm by an active load and it is current controlled. The reference voltage signals in the ( $\alpha\beta$ ) frame are used to evaluate the effectiveness of the voltage error compensation. First, the behavior of the MC is investigated when the error compensation is off. As can be seen from Figs. 16 (a) and (b), the reference voltages are distorted. Then the compensation technique is enabled. It is shown in Figs. 17 (a) and (b) that using this method, the distorted voltage due to converter error is compensated and the reference voltage is sinusoidal.

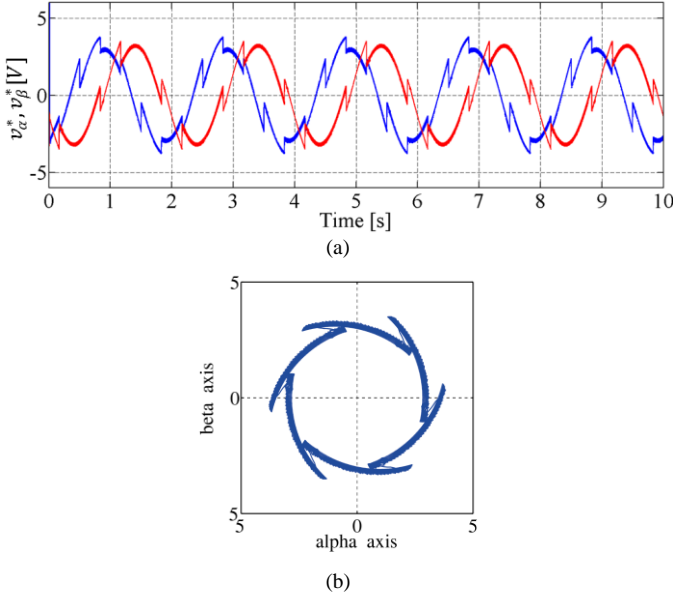


Fig. 16. Reference voltages in ( $\alpha$ - $\beta$ ) frame when compensation is OFF, at 15 rpm. a) Time waveforms; b) x-y representation.

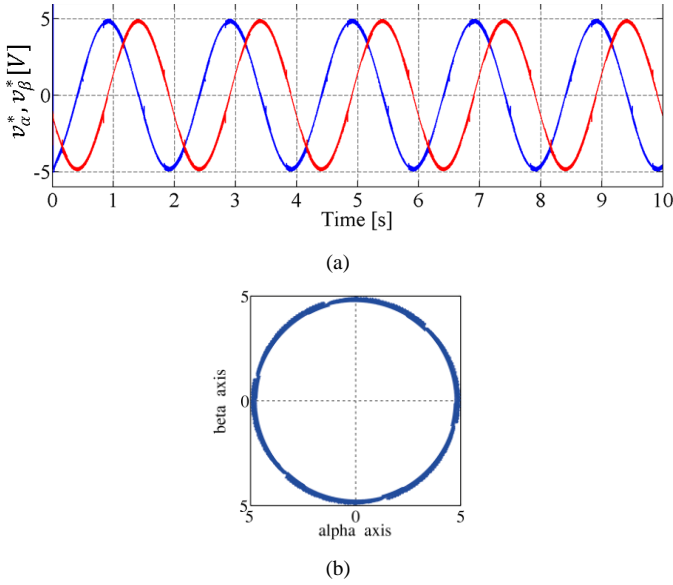


Fig. 17. Reference voltages in ( $\alpha$ - $\beta$ ) frame when compensation is ON, at 15 rpm. a) Time waveforms; b) x-y representation.

### C. Experimental Results

In this section, experimental results are presented for the part of identification of matrix converter nonlinear errors. A prototype of three-phase to three-phase matrix converter has been used to show the validity of the presented method. The control algorithm is implemented on the platform TMSF2812, a fixed point digital signal processor produced by Texas Instruments. The switching frequency is 8 kHz and the commutation is a current-based four-step commutation. Also, double-sided switching pattern is adopted.

The input phase voltage of matrix converter is 57.7 V. The motor and MC under test are described in Tables III and IV, respectively.

As shown in Fig. 18, two dc pulses with different amplitudes,  $I_{dc1} = 2$  A and  $I_{dc2} = 4$  A, are injected into the induction motor. The first dc level is injected in the time interval of 0 – 2 s and the second one is applied in the time interval 2–4 s. For the first test,  $v_{\alpha1}^*$  is sampled from  $t=1$  s to  $t=2$  s and for the second test,  $v_{\alpha2}^*$  is sampled from 3s to 4s as depicted in Fig. 19. It can be seen from this figure that,  $v_{\alpha1,avg}^*$  is ready at 2 s and  $v_{\alpha2,avg}^*$  is ready at 4 s. Then,  $R_d + R_s$  is identified by using (13) as shown in Fig. 20, leading to a value of 3.1  $\Omega$ . The threshold voltage is obtained via (14). The average value of actual threshold voltage  $V_{th}'$  of the considered converter is approximately 1.7 V as shown in Fig. 21. The positive value of identified  $V_{th}'$  means that the voltage drop effect is more important than the edge uncertainty effect. Because in this case, the input phase voltage is low (57.7 V) and therefore, the edge uncertainty effect would be low.

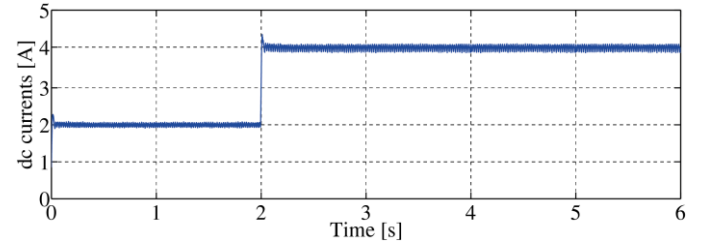


Fig. 18. Injected dc currents ( $I_{\alpha1}$  &  $I_{\alpha2}$ ).

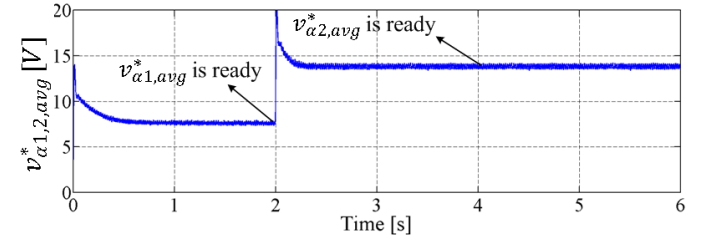


Fig. 19.  $v_{\alpha1}^*$  and  $v_{\alpha2}^*$  during the injection of  $I_{\alpha1}$  &  $I_{\alpha2}$ .

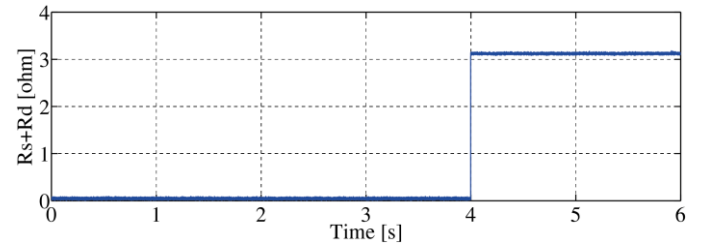


Fig. 20. Identification of overall resistance ( $R_s + R_d$ ).

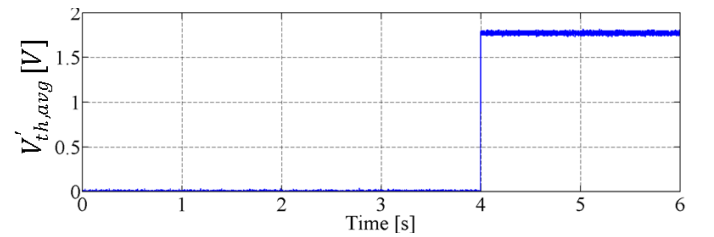


Fig. 21. Identification process for threshold voltage error.

## VI. CONCLUSION

This paper presents a simple self-commissioning algorithm for the identification of matrix converter nonlinear errors. The identification process is launched before the drive start-up and does not require off-line data manipulation, and neither use the knowledge of power device data from datasheets. The proposed method has been implemented on a current controlled synchronous reluctance motor in simulation and on an induction motor in experiments. Simulation results show that both the identification process and compensation process are effective.

## REFERENCES

- [1] Wheeler, P.W.; Rodriguez, J.; Clare, J.C.; Empringham, L.; Weinstein, A., "Matrix converters: a technology review," *Industrial Electronics, IEEE Transactions on*, vol.49, no.2, pp.276,288, Apr 2002.
- [2] Rixin Lai; Fei Wang; Burgos, R.; Yunqing Pei; Boroyevich, D.; Bingsen Wang; Lipo, T.A.; Immanuel, V.D.; Karimi, K.J., "A Systematic Topology Evaluation Methodology for High-Density Three-Phase PWM AC-AC Converters," *Power Electronics, IEEE Transactions on*, vol.23, no.6, pp.2665,2680, Nov. 2008.
- [3] Casadei, D.; Serra, G.; Tani, A., "The use of matrix converters in direct torque control of induction machines," *Industrial Electronics, IEEE Transactions on*, vol.48, no.6, pp.1057,1064, Dec 2001.
- [4] Rodriguez, J.; Rivera, M.; Kolar, J.W.; Wheeler, P.W., "A Review of Control and Modulation Methods for Matrix Converters," *Industrial Electronics, IEEE Transactions on*, vol.59, no.1, pp.58,70, Jan. 2012.
- [5] Kolar, J.W.; Friedli, T.; Rodriguez, J.; Wheeler, P.W., "Review of Three-Phase PWM AC-AC Converter Topologies," *Industrial Electronics, IEEE Transactions on*, vol.58, no.11, pp.4988,5006, Nov. 2011.
- [6] Friedli, T.; Kolar, J.W.; Rodriguez, J.; Wheeler, P.W., "Comparative Evaluation of Three-Phase AC-AC Matrix Converter and Voltage DC-Link Back-to-Back Converter Systems," *Industrial Electronics, IEEE Transactions on*, vol.59, no.12, pp.4487,4510, Dec. 2012.
- [7] Arias, A.; Silva, C.A.; Asher, G.M.; Clare, J.C.; Wheeler, P.W., "Use of a matrix converter to enhance the sensorless control of a surface-mount permanent-magnet AC motor at zero and low frequency," *Industrial Electronics, IEEE Transactions on*, vol.53, no.2, pp.440,449, April 2006.
- [8] Dan Xiao; Rahman, M.F., "Sensorless Direct Torque and Flux Controlled IPM Synchronous Machine Fed by Matrix Converter Over a Wide Speed Range," *Industrial Informatics, IEEE Transactions on*, vol.9, no.4, pp.1855,1867, Nov. 2013.
- [9] Reusser, C.A.; Silva, C.A.; Dominguez, P., "Low frequency sensorless Field Oriented Control of an induction machine fed by a direct matrix converter," *Industrial Electronics Society, IECON 2013 - 39th Annual Conference of the IEEE*, vol., no., pp.4874,4879, 10-13 Nov. 2013.
- [10] Jong-Woo Choi; Seung-Ki Sul, "Inverter output voltage synthesis using novel dead time compensation," *Power Electronics, IEEE Transactions on*, vol.11, no.2, pp.221,227, Mar 1996.
- [11] Holtz, J.; Juntao Quan, "Drift- and parameter-compensated flux estimator for persistent zero-stator-frequency operation of sensorless-controlled induction motors," *Industry Applications, IEEE Transactions on*, vol.39, no.4, pp.1052,1060, July-Aug. 2003.
- [12] Pellegrino, G.; Guglielmi, P.; Armando, E.; Bojoi, R.I., "Self-Commissioning Algorithm for Inverter Nonlinearity Compensation in Sensorless Induction Motor Drives," *Industry Applications, IEEE Transactions on*, vol.46, no.4, pp.1416,1424, July-Aug. 2010.
- [13] Kyo-Beum Lee; Blaabjerg, F., "A nonlinearity compensation method for a matrix converter drive," *Power Electronics Letters, IEEE*, vol.3, no.1, pp.19,23, March 2005.
- [14] Arias, A.; Empringham, L.; Asher, G.M.; Wheeler, P.W.; Bland, M.; Apap, M.; Sumner, M.; Clare, J.C., "Elimination of Waveform Distortions in Matrix Converters Using a New Dual Compensation Method," *Industrial Electronics, IEEE Transactions on*, vol.54, no.4, pp.2079,2087, Aug. 2007.
- [15] Huber, L.; Boroyevic, D., "Space vector modulated three-phase to three-phase matrix converter with input power factor correction," *Industry Applications, IEEE Transactions on*, vol.31, no.6, pp.1234,1246, Nov/Dec 1995.
- [16] Wheeler, P.W.; Clare, J.C.; Empringham, L.; Bland, M.; Kerris, K.G., "Matrix converters," *Industry Applications Magazine, IEEE*, vol.10, no.1, pp.59,65, Jan-Feb 2004.
- [17] Casadei, D.; Serra, G.; Tani, A.; Zarri, L., "Matrix converter modulation strategies: a new general approach based on space-vector representation of the switch state," *Industrial Electronics, IEEE Transactions on*, vol.49, no.2, pp.370,381, Apr 2002.